Editors' Suggestion

Spectroscopic Evidence of Kondo-Induced Quasiquartet in CeRh$_2$As$_2$

Denise S. Christovam[1,*] Miguel Ferreira-Carvalho[1,2] Andrea Marino,[1] Martin Sundermann,[3,1] Daisuke Takegami[1,]
Anna Melendez-Sans[1] Ku Ding Tsuei,[4] Zhiwei Hu,[1] Sahana Rößler[1] Manuel Valvidares[5] Maurits W. Haverkort,[6]
Yu Liu[7,‡] Eric D. Bauer[7] Liu Hao Tjeng[1] Gertrud Zwicknagl[8,1] and Andrea Severing[2,1,†]

[1]*Max Planck Institute for Chemical Physics of Solids, Nöthnitzer Straße 40, 01187 Dresden, Germany*
[2]*Institute of Physics II, University of Cologne, Zülpicher Straße 77, 50937 Cologne, Germany*
[3]*PETRA III, Deutsches Elektronen-Synchrotron DESY, Notkestraße 85, 22607 Hamburg, Germany*
[4]*National Synchrotron Radiation Research Center, 101 Hsin-Ann Road, Hsinchu 30077, Taiwan*
[5]*ALBA Synchrotron Light Source, Cerdanyola del Valles, Barcelona 08290, Spain*
[6]*Institute for Theoretical Physics, Heidelberg University,*
Philosophenweg 19, 69120 Heidelberg, Germany
[7]*Los Alamos National Laboratory, Los Alamos, New Mexico 87545, USA*
[8]*Technische Universität Braunschweig, 38106 Braunschweig, Germany*

CeRh$_2$As$_2$ is a new multiphase superconductor with strong suggestions for an additional itinerant multipolar ordered phase. The modeling of the low-temperature properties of this heavy-fermion compound requires a quartet Ce^{3+} crystal-field ground state. Here, we provide the evidence for the formation of such a quartet state using x-ray spectroscopy. Core-level photoelectron and x-ray absorption spectroscopy confirm the presence of Kondo hybridization in CeRh$_2$As$_2$. The temperature dependence of the linear dichroism unambiguously reveals the impact of Kondo physics for coupling the Kramer's doublets into an effective quasiquartet. Nonresonant inelastic x-ray scattering data find that the $|\Gamma_7^-\rangle$ state with its lobes along the 110 direction of the tetragonal structure (xy orientation) contributes most to the multiorbital ground state of CeRh$_2$As$_2$.

Characterizing novel ordering and understanding how they arise is key for the development of functional materials. Heavy-fermion materials have been important model systems for the discovery of novel phases as well as their cooperation, coexistence, or competition. This is due to the fact that the characteristic energy scale of these materials is of the order of a few meV which, in turn, implies a high tunability of the electronic properties [1–5]. CeRh$_2$As$_2$ is a heavy-fermion system of high current interest, experimentally [6–11] as well as theoretically [12–21]. This material exhibits multiphase unconventional superconductivity (SC) [22,23] and putative itinerant multipolar order; there are indications for a quadrupolar density wave below $T_0 = 0.48$ K and above the superconducting transition at $T_{SC} \approx 0.31$ K; the transition temperatures refer to newer sample generations [24]. The unusual behavior of CeRh$_2$As$_2$ is due to the presence of $4f$ electrons. This conclusion is derived from the properties of its non-f reference compound LaRh$_2$As$_2$ that can be quantitatively described by standard Eliashberg theory of strong-coupling electron-phonon superconductors [25]. For understanding the low-temperature (T) phases of CeRh$_2$As$_2$, it is also crucial that its f electrons form a quasiquartet ground state.

In the heavy-fermion state, the $4f$ degrees of freedom form heavy quasiparticles due to the Kondo effect (cf hybridization). CeRh$_2$As$_2$ forms in the globally centrosymmetric tetragonal CaBe$_2$Ge$_2$ structure with two identical Ce sites per unit cell. The Ce sites lack inversion symmetry so that the local point symmetry is C$_{4v}$ but the crystal-field split Ce^{3+} Hund's rule ground state of Ce^{3+} may be treated like D$_{4h}$, because the contribution of $5d$ states is negligible. Accordingly, the three Kramer's doublets can be written in J_z formalism as $|\Gamma_7^-\rangle = \sqrt{1-\alpha^2} \cdot |\pm 3/2\rangle - |\alpha| \cdot |\mp 5/2\rangle$, $|\Gamma_6\rangle = |\pm 1/2\rangle$, and $|\Gamma_7^+\rangle = \sqrt{1-\alpha^2} \cdot |\pm 5/2\rangle + |\alpha| \cdot |\mp 3/2\rangle$, and the f contribution to the quasiparticles has the character of the crystal-field ground state when the excited states are well separated from the ground state. However, if the system presents a Kondo temperature T_K of the order of magnitude of crystal-field splitting energies Δ_i, one may expect the Kondo effect to induce an effective quasiquartet ground state. Its character reflects both states of the quasiquartet.

The conjecture of a Kondo-induced quasiquartet is at the heart of renormalized band structure calculations in Ref. [9] that find superconductivity and other types of order may exist at different sites of the Fermi surface. Here, we investigate the electronic structure of Ce in CeRh$_2$As$_2$ in order to find spectroscopic evidence for such a quasiquartet. Core-level photoelectron spectroscopy with hard x rays (HAXPES) is sensitive to covalence and, hence, to the filling n_f of the Ce $4f$ shell [26–29]. Also, x-ray absorption spectroscopy (XAS) at the Ce $M_{4,5}$ edges can reveal signatures of hybridization effects by exhibiting, in addition to the main transition $3d^{10}4f^1 \to 3d^94f^2$, a satellite induced by hybridization with the $3d^{10}4f^0$ configuration [26,27,30]. The linear dichroism (LD) of XAS at the Ce $M_{4,5}$ edges, on the other hand, is sensitive to the symmetry of the crystal-field ground state when exploiting the dipole selection rules of linear polarized light [30,31]; at low T, the ground state is probed and excited states contribute to the net dichroism when they are populated thermally. This way, the T dependence of the LD provides insight into the sequence of crystal-field states and size of the crystal-field splitting energies $\Delta_{1,2}$. Nonresonant inelastic x-ray scattering (NIXS) is also sensitive to the crystal-field ground state, but it is based on multipole selection rules [32–36]. In NIXS, the direction of the momentum transfer with respect to the sample orientation takes over the role of the electric field vector in XAS. In contrast to XAS, NIXS is also sensitive to anisotropies with fourfold rotational symmetry, so that the orientation of, e.g., a $|\Gamma_7^\pm\rangle$ charge density within the tetragonal unit cell can be determined.

In the present Letter, we report results of HAXPES as well as XAS and NIXS measurements of CeRh$_2$As$_2$ single crystals. The spectra are analyzed with a full multiplet calculation to gain insight into the electronic structure of the crystal-field split Hund's rule ground state of Ce^{3+}. We use a simplified Anderson impurity calculation (SIAM) in the noncrossing approximation (NCA) to show that, in the presence of the Kondo effect and in the case $T_K \approx \Delta_i$, the excited crystal-field states do contribute to the LD also at low temperatures.

Growth and characterization of single crystalline CeRh$_2$As$_2$ are described in Supplemental Material [37]. The transition temperatures are $T_{SC} = 0.30$ K and $T_0 = 0.45$ K, which are in very good agreement with the values reported for newer generations of samples [24].

XAS spectra at the Ce $M_{4,5}$ edges (880–904 eV) were measured in the total electron yield mode at beam line BL29 BOREAS at ALBA synchrotron, Spain [38], with an energy resolution of 300 meV. Clean sample surfaces were obtained by cleaving the CeRh$_2$As$_2$ single crystals *in situ* in an ultrahigh vacuum of about 1×10^{-9} mbar prior to inserting them into the main chamber with a base pressure of 10^{-10} mbar. XAS data were taken at 3, 50, 100, and 200 K with the electric field $\vec{E} \| ab$ and $\vec{E} \| c$. NIXS experiments were performed at the Max-Planck NIXS

end station P01 at PETRA III/DESY, Germany, at 8 K with the same setup as described in Ref. [39]. The average momentum transfer amounted to $|\vec{q}| = 9.6 \pm 0.1$ Å^{-1}. The $N_{4,5}$ edges were measured with the momentum transfer $\vec{q}$ parallel to [100], [110], and [001]. HAXPES experiments were carried out at the Max-Planck-NSRRC HAXPES end station at the Taiwan undulator beam line BL12XU at SPring-8, Japan, with a photon energy of about 6.5 keV, an overall energy resolution of 250 meV, and a sample temperature of 40 K [40]. Samples were polished *in situ* in order to expose a fresh layer, and wide scans were performed to ensure the absence of O and C $1s$ signal from surface contamination or oxidation. The pressure in the main chamber was in the low 10^{-10} mbar. More information about the experimental setups can be found in Supplemental Material [37].

XAS and NIXS data are simulated with the full multiplet code QUANTY [41], starting with atomic parameters from the COWAN code [42] and applying typical reductions for the respective Hartree-Fock values of the Slater integrals and spin orbit values [43] (see Supplemental Material [37]). The reduction factors were optimized to best reproduce the isotropic spectrum in the case of XAS [31] and (pseudo)isotropic for NIXS. Both are constructed from the directional-dependent data $[I_{iso} = (2I_{\|ab} + I_{\|c})/3]$. Furthermore, a Gaussian and Lorentzian broadening are applied to account for resolution and lifetime effects (see Supplemental Material [37]).

Figure 1(a) shows the Ce $3d$ core-level HAXPES data of CeRh$_2$As$_2$ without any background correction. CeRh$_2$As$_2$ shows the three spectral weights that arise in the presence of the core hole, when the ground state is a coherent interference of the $4f^0$, $4f^1$, and $4f^2$ configurations [28]. Also, the *isotropic* XAS spectrum, shown in Fig. 1(b), reveals the presence of a $4f$ configuration different from $4f^1$. The spectral weights corresponding to the $3d^{10}4f^0 \to 3d^94f^1$ transition show up as small satellites on the high-energy tails of the M_5 and M_4 absorption lines, shown on an enlarged scale in the inset. These small intensities originating from the $4f^0$ configuration confirm that the Kondo effect is indeed present in CeRh$_2$As$_2$, an aspect that turns out to be crucial for the analysis of the temperature dependence of the linear dichroism in the XAS spectra as discussed below.

The top spectra in Fig. 2 show the polarization-dependent XAS data of CeRh$_2$As$_2$ at 3 K (red and blue circles) and at the bottom the experimental linear dichroism LD $= I_{E\|c} - I_{E\|ab}$ 5 times enlarged (purple circles). At first, we compare the data with the simulations of the pure $|\pm J_z\rangle$ states of the f^1 configuration that are displayed in the inset. Obviously, a pure $|\pm 5/2\rangle$ and $|\pm 1/2\rangle$ can be excluded as ground state. The pure $|\pm 3/2\rangle$ may resemble the data best, but, as we will explain below, we will need to consider not only the correct crystal-field scheme, but also the Kondo effect. We note that the measured dichroic signal is
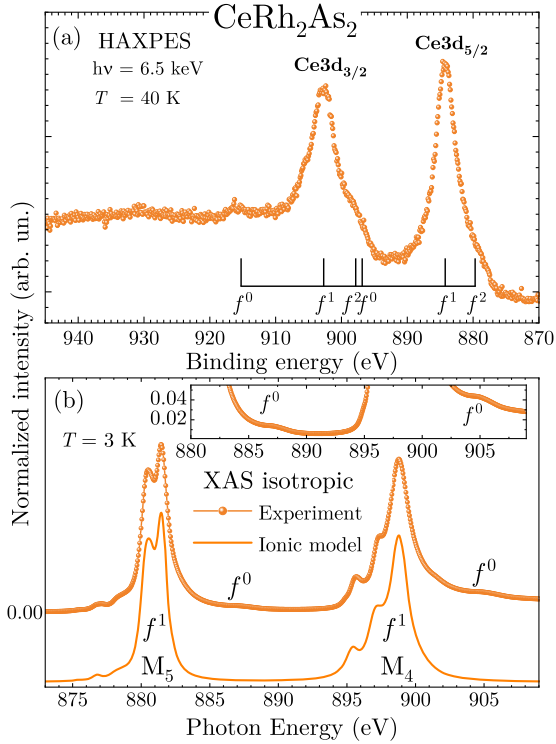
FIG. 1.   (a) Ce $3d$ core level HAXPES data of CeRh$_2$As$_2$. The black ruler at the bottom indicates the position of the f^0, f^1, and f^2 spectral weights. (b) Isotropic XAS spectrum of CeRh$_2$As$_2$ (dots) and the corresponding ionic multiplet simulation of the f^1 configuration (solid line). The inset shows a close-up to the energy regions with the f^0 satellites.

relatively small, and we verify its reliability by analyzing the line shape. We recall that the line shape of the $M_{4,5}$ dichroism of Ce^{3+} ions is unique as long as the crystal-field splitting is negligible compared to the inverse lifetime of the $M_{4,5}$ white lines; see Refs. [44,45]. After optimizing the reduction factors by means of the isotropic spectrum [see Fig. 1(b)], we plot this unique line shape on top of the measured dichroic spectrum, and we indeed conclude that the experimental features all belong to a Ce^{3+} ion in the small crystal-field limit. Also, the corresponding simulations for the $M_{4,5}$ spectra match the measured ones excellently.

The temperature dependence of the LD(T) at the M_5 and M_4 edges is shown on an expanded energy scale in Fig. 3(a) for 3, 50, 100, and 200 K. The LD at 50 K has increased with respect to 3 K, as indicated by the arrows. The change in LD(T) indicates that an excited crystal-field state is close. LD(T) remains almost as large at 100 K and then decreases when warming up to 200 K. Also, here it is informative to understand the T dependence of the LD by looking at first at the pure $|\pm J_z\rangle$ states that are depicted in the inset in Fig. 2. The $|\pm 1/2\rangle$ has a stronger dichroism of the same sign as the one at 3 K, whereas the LD of the $|\pm 5/2\rangle$ state is large and opposite. Hence, the increase of
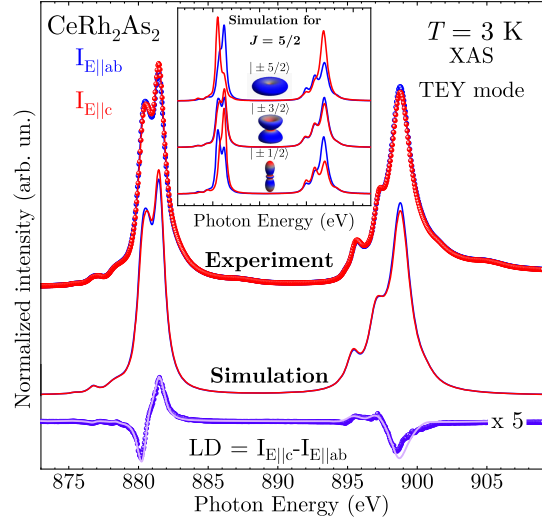
the LD(T) when warming up to 50 K must be due to the increasing population of the $|\Gamma_6\rangle = |\pm 1/2\rangle$ state, followed by the successive population of the second $|\Gamma_7^\mp\rangle$ state of majority $|\pm 5/2\rangle$ that compensates the LD of the $|\Gamma_6\rangle$ when warming up further to 100 and 200 K.

First, we simulate LD(T) by assuming the crystal-field model that satisfies the macroscopic data best, especially the high-temperature anisotropy of the static susceptibility where the impact of the Kondo effect can be neglected. Hafner *et al.* [9] propose the sequence of states that we obtain from the above comparison with the pure $|J_z\rangle$ states, with $\Delta_1 = 30$ K, $\Delta_2 = 180$ K, and $\alpha = 0.48$ for the crystal-field splittings and mixing factor of the ground state, respectively. These numbers are based on the analysis of the specific heat and static susceptibility. This model reproduces qualitatively LD(T) at 50, 100, and 200 K when taking into account the respective Boltzmann occupations of the excited states [see Fig. 3(b)]. It contradicts, however, the experiment at low temperatures where the Kondo effect starts to manifest: At 3 K, the simulated LD turns out to be opposite to the experimental one [compare Figs. 3(a) and 3(b)].

We take the discrepancy between data and crystal-field simulation of LD(T) at low T as a strong suggestion for having to consider the impact of the Kondo interaction, since Kondo is a low-T effect. The SIAM/NCA calculations [45–47] take into account the hybridization of the three crystal-field states with the conduction electron bath. It turns out that the Kondo effect induces a finite occupation of the first and second excited crystal-field states also at 3 K, in contrast to the Boltzmann occupations, where only the
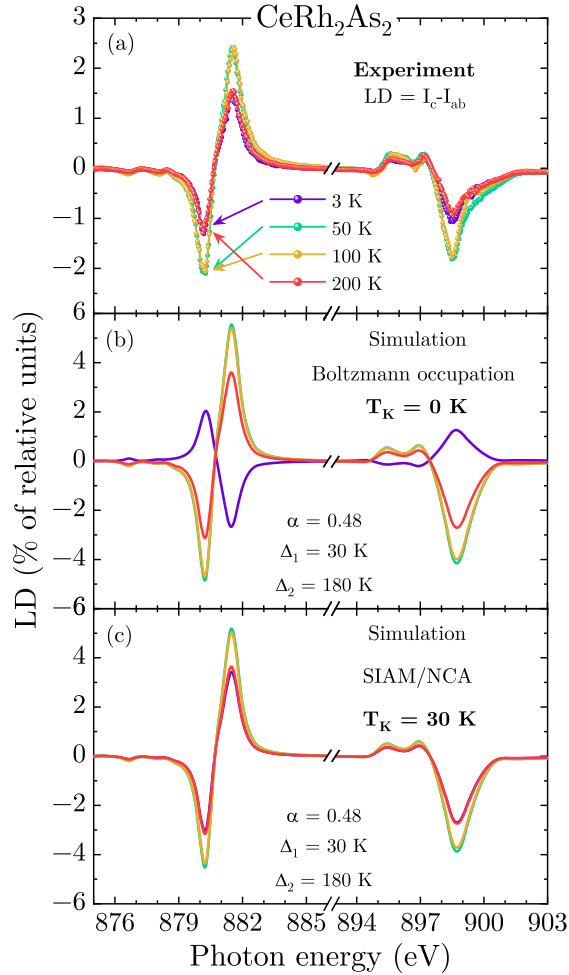

FIG. 2.   Linear polarized XAS spectra of CeRh$_2$As$_2$ at 3 K for the electric field vector $\vec{E}\|c$ (red line) and $\vec{E}\|ab$ plane (blue line) and linear dichroism (purple line); dots are for the experiment, and lines are the full multiplet simulation of the f^1 configuration. The inset shows the calculated individual contributions to each pure $|\pm J_z\rangle$ state.

FIG. 3. (a) Measured T dependence of the LD at $T = 3$ (purple line), 50 (green line), 100 (yellow line), and 200 K (red line). The panels below show two different simulations: an ionic crystal-field calculation considering the Boltzmann occupation of excited states but no Kondo effect (b) and the same crystal-field model including the Kondo effect (c); see the text. The scale was multiplied by 100 to show the percentage of LD.

lowest state is occupied. The Kondo-induced (solid lines) and Boltzmann-only (dashed lines) occupations as a function of T are displayed in Fig. 4(a). The SIAM/NCA calculations take into account the same crystal-field model as above and a Kondo temperature T_K of 30 K. The latter is suggested from macroscopic data [6,9]. The Kondo-mixed ground state at low T is calculated with a $4f$-shell occupation of $n_f^{tot} = 95\%$. Beginning at 50 K, but certainly at 100 K, the differences between Kondo-induced and Boltzmann-only occupation are negligible. Therefore, the Kondo effect has the strongest impact on the simulated $LD(T)$ at 3 K: Because of the Kondo-induced contribution of the higher-lying states, the sign of the LD at 3 K is now correctly reproduced [see Fig. 3(c)].

The calculation of the entropy within the SIAM/NCA model based on the above crystal-field scheme and Kondo

temperature yields the red line in Fig. 4(c), which reproduces $R \ln 4$ at about 60 K very well, and it is in good agreement with the analysis of the experimental specific heat (blue dots) by Khim *et al.* [6].

While a T_K of 30 K reproduces $LD(T)$ well, we show in Supplemental Material analyses with other T_K values [37]. We find that a lower value of $T_K = 15$ K still produces the wrong sign in the LD at 3 K; see Fig. S1 [37]. This indicates that $k_B T_K$ must be at least of the same order of magnitude as the crystal-field splitting, thus implying that the degeneracy of the relevant low-energy subspace is effectively higher than twofold. We also find that the entropy sets limits on the upper and lower value of T_K; see Fig. S2 [37].

$LD(T)$ is well described with a $|\Gamma_7^\pm\rangle$ lowest in energy. It is, however, not yet clear whether it is the $|\Gamma_7^+\rangle$ $(x^2 - y^2)$ or the $|\Gamma_7^-\rangle$ $(xy$ orientation). We address this question with directional-dependent NIXS. NIXS spectra at 8 K for momentum transfers $\vec{q}\|(100)$, $\vec{q}\|(110)$, and for completeness also $\vec{q}\|(001)$ are displayed in Fig. 5. The spectra are normalized to the integral of the Compton background at higher energy transfers, and a linear background is subtracted as described in Supplemental Material and displayed in Fig. S3 [37]. The directional dependence in the ab plane is fairly weak, except for a more distinct region at around 105 eV energy transfer. The in-plane directional dependence gives the desired information about the sign of the $|\Gamma_7^\pm\rangle$ state. The 45° rotation would imply a switch in intensity of the (100) (blue) and (110) (green) signals. Also, the NIXS spectra were simulated with the Kondo-mixed ground state $|GS_{Kondo}\rangle$, using the respective occupations at 8 K. The Kondo mixing of states reduces and alters slightly the directional dependence in the ab plane with respect to pure $|\Gamma_7^\pm\rangle$ states (see Fig. S4 in Supplemental Material [37]) due to the admixture of the rotational invariant $|\Gamma_6\rangle$ and the excited $|\Gamma_7^\mp\rangle$ state with lobes rotated by 45° and, consequently, an opposite in-plane anisotropy. The resulting NIXS simulation with the orbital mixed ground state $|GS_{Kondo}\rangle$ shows that the lobes are along (110), thus confirming the $|\Gamma_7^-\rangle$ state must be the one most strongly occupied. A more detailed discussion about the NIXS spectra is found in Supplemental Material [37].

Putting together the results of macroscopic data and the present T-dependent XAS and low-T NIXS, we find that the $4f^1$ part of the multiorbital ground-state wave function with $n_f^{tot} = 0.95$ consists of $\sqrt{0.58}|\Gamma_7^-\rangle$, $\sqrt{0.29}|\Gamma_6\rangle$, and $\sqrt{0.08}|\Gamma_7^+\rangle$ with $|\Gamma_7^-\rangle = 0.88|\pm 3/2\rangle - 0.48|\mp 5/2\rangle$, $|\Gamma_7^+\rangle = 0.48|\pm 3/2\rangle + 0.88|\mp 5/2\rangle$, and $\Gamma_6\rangle = |\pm 1/2\rangle$. The corresponding charge density is displayed in Figs. 4(b) and 5. The dominance of the $|\Gamma_7^-\rangle$ state accommodates very well the Fermi surface as calculated in Ref. [9].

Quantitatively, the present simulation overestimates the T dependence of $LD(T)$. This is most likely due to the fact that the present SIAM/NCA model is too simplistic. For example, the calculations performed on the NCA frame are
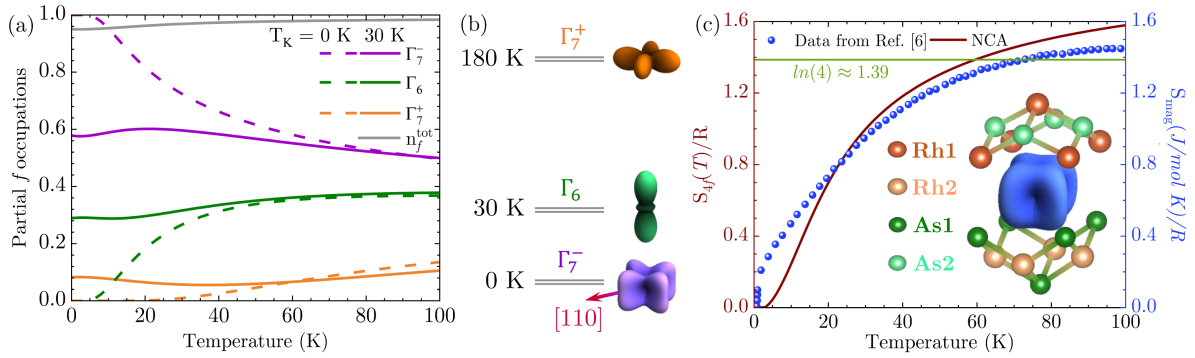
FIG. 4. (a) SIAM/NCA calculation of partial $4f$ occupations for $T_K = 30$ K (solid lines) and Boltzmann statistics ($T_K = 0$, dashed lines) for the crystal-field scheme according Ref. [9], shown in (b), with $|\Gamma_7^-\rangle = 0.88| \pm 3/2\rangle - 0.48| \mp 5/2\rangle$, $|\Gamma_6\rangle = | \pm 1/2\rangle$, and $|\Gamma_7^+\rangle = 0.88| \pm 5/2\rangle + 0.48| \mp 3/2\rangle$. (c) SIAM/NCA calculated entropy as a function of the temperature (red solid line) compared to specific heat data from Ref. [6] (blue dots) and expected entropy of a quartet (horizontal green line). Inset: Ce charge density of the Kondo-mixed ground state (58% $|\Gamma_7^-\rangle$, 29% $|\Gamma_6\rangle$, and 8% $|\Gamma_7^+\rangle$) with its nearest neighbors.

in the limit U $\to \infty$, meaning they do not take into account the influence of the $4f^2$ configuration and all weight is concentrated on $4f^1$. Moreover, symmetry-dependent hybridization is not taken into account, although renormalized band structure calculations that do consider symmetries [48] show that the $|\Gamma_7^+\rangle$ at 180 K contributes significantly to the Fermi surface—actually, more than expected from an isotropic calculation (see Fig. S5 in Supplemental Material [37]).

In summary, the presence of significant cf hybridization in CeRh$_2$As$_2$ is consistent with core-level HAXPES and M-edge XAS data. The temperature dependence of the linear dichroism LD(T) in M-edge XAS is qualitatively

reproduced with the crystal-field model that was suggested from the anisotropy of the static susceptibility and the specific heat when taking into account the Kondo-induced coupling of all crystal-field states to the conduction electron bath. The resulting multiorbital ground state is an effective quartet that reproduces well the asymptotic value of entropy from the specific heat, thus validating the conjecture of a quasiquartet ground state that is crucial for superconductivity to coexist with other types of order.

FIG. 5. Normalized and background-corrected NIXS data for **q**$\|$[001] (red), **q**$\|$[110] (green), and **q**$\|$[100] (blue). The lines represent the simulation in the SIAM/NCA work frame for $|GS_{Kondo}\rangle$ ground state, with the $|\Gamma_7^-\rangle$ most strongly occupied. The inset represent the respective orbital orientation within the ab plane.

*Correlspnding author: denise.christovam@cpfs.mpg.de
†Correlspnding author: severing@ph2.uni-koeln.de
‡Present address: Center for Correlated Matter and Department of Physics, Zhejiang University, Hangzhou 310058, China.

[1] J. Flouquet, *Progress in Low Temperature Physics*, edited by W. P. Halperin (Elsevier, New York, 2005), Vol. XV, pp. 139–268, On the Heavy Fermion Road.
[2] P. Thalmeier and G. Zwicknagl, *Handbook on the Physics and Chemistry of Rare Earths*, edited by

J.-C. B. K. A. Gschneidner, Jr. and V. Pecharsky (Elsevier, New York, 2005), Vol. 34, pp. 139–268.

[3] P. Fulde, P. Thalmeier, and G. Zwicknagl, *Solid State Physics*, edited by H. Ehrenreich and F. Spaepen (Elsevier, 2006), Vol. 60, p. 1, Strongly correlated electrons.

[4] P. Coleman, *Handbook of Magnetism and Advance Magnetic Materials*, edited by H. Kronmüller, S. Parkin, and I. Zutic (John Wiley and Sons, New York, 2007), Vol. 1, pp. 95–148, Heavy Fermions: Electrons at the Edge of Magnetism.

[5] D. I. Khomskii, *Basic Aspects of the Quantum Theory of Solids* (Cambridge University Press, Cambridge, England, 2010).

[6] S. Khim, J. F. Landaeta, J. Banda, N. Bannor, M. Brando, P. M. R. Brydon, D. Hafner, R. Küchler, R. Cardoso-Gil, U. Stockert, A. P. Mackenzie, D. F. Agterberg, C. Geibel, and E. Hassinger, Field-induced transition within the superconducting state of $CeRh_2As_2$, Science **373**, 1012 (2021).

[7] S. I. Kimura, J. Sichelschmidt, and S. Khim, Optical study of the electronic structure of locally noncentrosymmetric $CeRh_2As_2$, Phys. Rev. B **104**, 245116 (2021).

[8] M. Kibune, S. Kitagawa, K. Kinjo, S. Ogata, M. Manago, T. Taniguchi, K. Ishida, M. Brando, E. Hassinger, H. Rosner, C. Geibel, and S. Khim, Observation of antiferromagnetic order as odd-parity multipoles inside the superconducting phase in $CeRh_2As_2$, Phys. Rev. Lett. **128**, 057002 (2022).

[9] D. Hafner, P. Khanenko, E.-O. Eljaouhari, R. Küchler, J. Banda, N. Bannor, T. Lühmann, J. F. Landaeta, S. Mishra, I. Sheikin, E. Hassinger, S. Khim, C. Geibel, G. Zwicknagl, and M. Brando, Possible quadrupole density wave in the superconducting Kondo lattice $CeRh_2As_2$, Phys. Rev. X **12**, 011023 (2022).

[10] J. F. Landaeta, P. Khanenko, D. C. Cavanagh, C. Geibel, S. Khim, S. Mishra, I. Sheikin, P. M. R. Brydon, D. F. Agterberg, M. Brando, and E. Hassinger, Field-angle dependence reveals odd-parity superconductivity in $CeRh_2As_2$, Phys. Rev. X **12**, 031001 (2022).

[11] S. Mishra, Y. Liu, E. D. Bauer, F. Ronning, and S. M. Thomas, Anisotropic magnetotransport properties of the heavy-fermion superconductor $CeRh_2As_2$, Phys. Rev. B **106**, L140502 (2022).

[12] D. Möckli and A. Ramires, Two scenarios for superconductivity in $CeRh_2As_2$, Phys. Rev. Res. **3**, 023204 (2021).

[13] E. G. Schertenleib, M. H. Fischer, and M. Sigrist, Unusual H-T phase diagram of $CeRh_2As_2$: The role of staggered noncentrosymmetricity, Phys. Rev. Res. **3**, 023179 (2021).

[14] A. Ptok, K. J. Kapcia, P. T. Jochym, J. Łażewski, A. M. Oleś, and P. Piekarz, Electronic and dynamical properties of $CeRh_2As_2$: Role of Rh_2As_2 layers and expected orbital order, Phys. Rev. B **104**, L041109 (2021).

[15] A. Skurativska, M. Sigrist, and M. H. Fischer, Spin response and topology of a staggered-Rashba superconductor, Phys. Rev. Res. **3**, 033133 (2021).

[16] K. Nogaki, A. Daido, J. Ishizuka, and Y. Yanase, Topological crystalline superconductivity in locally noncentrosymmetric $CeRh_2As_2$, Phys. Rev. Res. **3**, L032071 (2021).

[17] D. Möckli and A. Ramires, Superconductivity in disordered locally noncentrosymmetric materials: An application to $CeRh_2As_2$, Phys. Rev. B **104**, 134517 (2021).

[18] D. C. Cavanagh, T. Shishidou, M. Weinert, P. M. R. Brydon, and D. F. Agterberg, Nonsymmorphic symmetry and field-driven odd-parity pairing in $CeRh_2As_2$, Phys. Rev. B **105**, L020505 (2022).

[19] K. Nogaki and Y. Yanase, Even-odd parity transition in strongly correlated locally noncentrosymmetric superconductors: Application to $CeRh_2As_2$, Phys. Rev. B **106**, L100504 (2022).

[20] K. Machida, Violation of Pauli-Clogston limit in the heavy-fermion superconductor $CeRh_2As_2$: Duality of itinerant and localized $4f$ electrons, Phys. Rev. B **106**, 184509 (2022).

[21] T. Hazra and P. Coleman, Triplet pairing mechanisms from Hund's-Kondo models: Applications to UTe_2 and $CeRh_2As_2$, Phys. Rev. Lett. **130**, 136002 (2023).

[22] A. Pourret and G. Knebel, Driving multiphase superconductivity, Science **373**, 962 (2021).

[23] E. M. Nica, S. Ran, L. Jiao, and Q. Si, Multiple superconducting phases in heavy-fermion metals, Front. Electron. Mater. **2**, 1 (2022).

[24] K. Semeniuk, D. Hafner, P. Khanenko, T. Lühmann, J. Banda, J. F. Landaeta, C. Geibel, S. Khim, E. Hassinger, and M. Brando, Decoupling multiphase superconductivity from normal state ordering in $CeRh_2As_2$, Phys. Rev. B **107**, L220504 (2023).

[25] J. F. Landaeta, A. M. León, S. Zwickel, T. Lühmann, M. Brando, C. Geibel, E.-O. Eljaouhari, H. Rosner, G. Zwicknagl, E. Hassinger, and S. Khim, Conventional type-II superconductivity in locally noncentrosymmetric $LaRh_2As_2$ single crystals, Phys. Rev. B **106**, 014506 (2022).

[26] O. Gunnarsson and K. Schönhammer, Electron spectroscopies for Ce compounds in the impurity model, Phys. Rev. B **28**, 4315 (1983).

[27] J. C. Fuggle, F. U. Hillebrecht, Z. Zołnierek, R. Lässer, C. Freiburg, O. Gunnarsson, and K. Schönhammer, Electronic structure of Ce and its intermetallic compounds, Phys. Rev. B **27**, 7330 (1983).

[28] O. Gunnarsson, K. Schönhammer, J. Allen, K. Karlsson, and O. Jepsen, Information from photoemission spectral weights and shapes, J. Electron Spectrosc. Relat. Phenom. **117–118**, 1 (2001).

[29] M. Sundermann *et al.*, Quantitative study of the f occupation in $CeMIn_5$ and other cerium compounds with hard x-rays, J. Electron Spectrosc. Relat. Phenom. **209**, 1 (2016).

[30] T. Willers *et al.*, Spectroscopic determination of crystal-field levels in $CeRh_2Si_2$ and $CeRu_2Si_2$ and of the $4f^0$ contributions in CeM_2Si_2 (M = Cu, Ru, Rh, Pd, and Au), Phys. Rev. B **85**, 035117 (2012).

[31] P. Hansmann, A. Severing, Z. Hu, M. W. Haverkort, C. F. Chang, S. Klein, A. Tanaka, H. H. Hsieh, H.-J. Lin, C. T. Chen, B. Fåk, P. Lejay, and L. H. Tjeng, Determining the crystal-field ground state in rare earth heavy fermion materials using soft-x-ray absorption spectroscopy, Phys. Rev. Lett. **100**, 066405 (2008).

[32] W. Schülke, *Electron Dynamics by Inelastic X-Ray Scattering*, Oxford Series on Synchrotron Radiation (Oxford, New York, 2007).

[33] R. A. Gordon, G. T. Seidler, T. T. Fister, M. W. Haverkort, G. A. Sawatzky, A. Tanaka, and T. K. Sham, High multipole

transitions in NIXS: Valence and hybridization in 4f systems, Europhys. Lett. **81**, 26004 (2008).

[34] R. A. Gordon, M. W. Haverkort, S. Sen Gupta, and G. A. Sawatzky, Orientation-dependent x-ray Raman scattering from cubic crystals: Natural linear dichroism in MnO and CeO_2, J. Phys. Conf. Ser. **190**, 012047 (2009).

[35] T. Willers, F. Strigari, N. Hiraoka, Y. Q. Cai, M. W. Haverkort, K.-D. Tsuei, Y. F. Liao, S. Seiro, C. Geibel, F. Steglich, L. H. Tjeng, and A. Severing, Determining the in-plane orientation of the ground-state orbital of $CeCu_2Si_2$, Phys. Rev. Lett. **109**, 046401 (2012).

[36] M. Sundermann, A. Amorese, F. Strigari, B. Leedahl, L. H. Tjeng, M. W. Haverkort, H. Gretarsson, H. Yavaş, M. M. Sala, E. D. Bauer, P. F. S. Rosa, J. D. Thompson, and A. Severing, Orientation of the ground-state orbital in $CeCoIn_5$ and $CeRhIn_5$, Phys. Rev. B **99**, 235143 (2019).

[37] See Supplemental Material at http://link.aps.org/supplemental/10.1103/PhysRevLett.132.046401 for additional information on experimental conditions, simulations, analysis of NIXS spectra, and how TK impacts the analysis of the linear dichroism and entropy.

[38] A. Barla, J. Nicolás, D. Cocco, S. M. Valvidares, J. Herrero-Martín, P. Gargiani, J. Moldes, C. Ruget, E. Pellegrin, and S. Ferrer, Design and performance of BOREAS, the beamline for resonant x-ray absorption and scattering experiments at the ALBA synchrotron light source, J. Synchrotron Radiat. **23**, 1507 (2016).

[39] M. Sundermann, K. Chen, H. Yavaş, H. Lee, Z. Fisk, M. W. Haverkort, L. H. Tjeng, and A. Severing, The quartet ground state in CeB_6: An inelastic x-ray scattering study, Europhys. Lett. **117**, 17003 (2017).

[40] J. Weinen, T. Koethe, C. Chang, S. Agrestini, D. Kasinathan, Y. Liao, H. Fujiwara, C. Schüßler-Langeheine, F. Strigari, T. Haupricht, G. Panaccione, F. Offi, G. Monaco, S. Huotari, K.-D. Tsuei, and L. Tjeng, Polarization dependent hard x-ray photoemission experiments for solids: Efficiency and limits for unraveling the orbital character of the valence band, J. Elecron. Spectrosc. Relat. Phenom. **198**, 6 (2015).

[41] M. W. Haverkort, QUANTY for core level spectroscopy—excitons, resonances and band excitations in time and frequency domain, J. Phys. Conf. Ser. **712**, 012001 (2016).

[42] R. Cowan, *The Theory of Atomic Structure and Spectra* (University of California, Berkeley, 1981).

[43] A. Tanaka and T. Jo, Resonant 3d, 3p and 3s photoemission in transition metal oxides predicted at 2p threshold, J. Phys. Soc. Jpn. **63**, 2788 (1994).

[44] M. Sundermann, F. Strigari, T. Willers, H. Winkler, A. Prokofiev, J. M. Ablett, J.-P. Rueff, D. Schmitz, E. Weschke, M. M. Sala, A. Al-Zein, A. Tanaka, M. W. Haverkort, D. Kasinathan, L. H. Tjeng, S. Paschen, and A. Severing, $CeRu_4Sn_6$: A strongly correlated material with nontrivial topology, Sci. Rep. **5**, 17937 (2015).

[45] A. Amorese, A. Marino, M. Sundermann, K. Chen, Z. Hu, T. Willers, F. Choueikani, P. Ohresser, J. Herrero-Martin, S. Agrestini, C. T. Chen, H.-J. Lin, M. W. Haverkort, S. Seiro, C. Geibel, F. Steglich, L. H. Tjeng, G. Zwicknagl, and A. Severing, Possible multiorbital ground state in $CeCu_2Si_2$, Phys. Rev. B **102**, 245146 (2020).

[46] V. Zevin, G. Zwicknagl, and P. Fulde, Temperature dependence of the 4f quadrupole moment of Yb in $YbCu2Si_2$, Phys. Rev. Lett. **60**, 2331 (1988).

[47] G. Zwicknagl, V. Zevin, and P. Fulde, Simple approximation scheme for the Anderson impurity Hamiltonian, Z. Phys. B Condens. Matter **97**, 365 (1990).

[48] G. Zwicknagl, Quasi-particles in heavy fermion systems, Adv. Phys. **41**, 203 (1992).